Textured Nd-Fe-B hard magnetic thin films prepared by pulsed laser deposition with single alloy targets

T. Nguyen Van, Isabelle Gomes De Moraes, Nora Dempsey, Corinne Champeaux, Frédéric Dumas-Bouchiat

Textured Nd-Fe-B hard magnetic thin films prepared by pulsed laser deposition with single alloy targets

T. Nguyen Van[1], I. de Moraes[2], N. M. Dempsey[2], C. Champeaux[1], F. Dumas-Bouchiat[1,*]

[1]Univ. Limoges, CNRS, IRCER, UMR 7315, 87068 Limoges, France,

[2]Univ. Grenoble Alpes, CNRS, Institut NEEL, 38000 Grenoble, France.

*Corresponding author: Frédéric Dumas-Bouchiat

Email: frederic.dumas-bouchiat@unilim.fr

Abstract: Nd-Fe-B thin films have been successfully developed by Pulsed Laser Deposition (PLD) onto silicon substrates. In order to explore the crucial role of target composition during PLD, five single alloy targets, representing specific atomic compositions (Nd/Fe atomic ratio varied in the range 0.18–0.47) have been tested and studied. In a determined deposition temperature range of 550°C-630°C, thin films made from a target with Nd/Fe=0.45 present the best hard magnetic properties, a quasi-single magnetic phase, both coercivity and remanence above 1 T and a square loop shape. FIB-EBS analyses associated with XRD, SEM and SQUID magnetic measurements indicate that the high values of both remanent magnetization and coercivity are ascribed to film texturation and to partial decoupling of the hard magnetic $Nd_2Fe_{14}B$ grains by a secondary Nd-rich phase. PLD performed with other target compositions and non-optimized deposition temperatures leads to poorer magnetic properties, owing to the presence of soft magnetic phase and non-textured or oxidized thin films.

Key words: Nd-Fe-B, hard magnetic thin film, pulsed laser deposition (PLD).

I. Introduction

Hard magnetic materials represent a key component of macroscopic electro-mechanical devices (e.g. wind turbines, hybrid-electric vehicles, air-conditioners) [1] and hold enormous potential for use at the microscale (micro-systems dedicated to telecommunications, internet of things (IoT) and bio-technology) [2,3]. Today's high performance magnets are based on rare earth - transition metal intermetallic phases [1], and the highest energy densities are achieved for magnets based on the tetragonal $Nd_2Fe_{14}B$ phase (maximum theoretical energy product $(B.H)_{max}$ = 512 kJ/m^3) [1,4,5]. Theoretical modelling suggests that the energy product can be significantly enhanced in nanocomposites which intimately combine a high coercivity hard phase with a high magnetization soft phase [6]. While both top-down [7] and bottom-up [8] techniques have been used to fabricate hard-soft nanocomposites, the reported energy products fall far short of predicted values. This is attributed to insufficient control of the dimensions of the soft magnetic phase, which according to modelling, should be no larger than twice the domain wall width, δ, of the hard phase (δ= 2.6, 3.9 and 4.5 nm for $SmCo_5$, $Nd_2Fe_{14}B$ and CoPt, respectively) [1]. Laser Vaporization Nanoparticle Sources (LVNS) have been used to prepare magnetic nanoparticles of diameter as low as 2 nm [9–11]. Reactors which combine a nanoparticle source with a film deposition source (e.g. Pulsed Laser Deposition (PLD) [12–14], or sputtering [15]) hold the potential to prepare hard-soft nanocomposites in which the size of soft nano-inclusions in a hard magnetic matrix can be restricted to below 10 nm. As a first step towards fabricating hard-soft nanocomposites with a reactor based on the association of a pulsed LVNS and a PLD system, here we report on the fabrication of NdFeB films by PLD. Literature reports on the fabrication of NdFeB films by PLD fall into two groups. The first deals with epitaxial growth using multiple targets (Nd, Fe, B,

or the combination of one of the two), on single crystalline Al_2O_3 or MgO substrates [16–18]. The second deals with films deposited using a single composite Nd-Fe-B target on tantalum or silicon substrates [19–22]. In the latter case films were either deposited at elevated temperatures or at room temperature and then annealed to crystallize the hard magnetic $Nd_2Fe_{14}B$ phase. Such films show isotropic magnetic properties, which limits the remanent magnetization values achievable, while out of plane anisotropy was achieved in the epitaxially grown films made with multiple targets. Though the use of multiple targets allows a fine tuning of the film composition, it requires ultra-high vacuum conditions in light of the susceptibility to oxidation of pure Nd and it adds complexity to the control of the PLD procedure. The use of a composite Nd-Fe-B target allows for simpler two-target PLD systems (Nd-Fe-B target and a buffer / capping layer target) and more tolerance on the base oxygen level, but testing of different target compositions is required to tune the film composition. It is known that Nd content in excess of that of the stoichiometric $Nd_2Fe_{14}B$ phase is required to induce coercivity in NdFeB magnets in bulk or film form. The excess Nd leads to the formation of a non-magnetic grain boundary phase that serves to magnetically decouple neighboring $Nd_2Fe_{14}B$ grains. Here we report on the fabrication of out-of-plane textured NdFeB films on thermally oxidized Si substrates by PLD with single composite alloy Nd-Fe-B targets.

II. Experimental details

A set of five composite targets were prepared by induction melting followed by casting into a Cu mould. The overall Nd/Fe atomic ratio was varied from target to target (#1 = 0.47, #2 = 0.45, #3 = 0.42, #4 = 0.33, #5 = 0.18) while the B/Nd ratio was kept constant (~0.5). Ta/Nd-Fe-B (~150 nm)/Ta tri-layers were grown by PLD on (001) silicon substrates thermally oxidized to a depth of 100 nm (the nominal thickness of the Ta layers was 50 nm). The role of the Ta underlayer is to prevent substrate-film interdiffusion. Moreover, Ta was shown to promote out-of-plane (oop) epitaxial growth of $Nd_2Fe_{14}B$ prepared by PLD or sputtering [17,18,23]. The role of the Ta capping layer is to protect the film from oxidation. The base pressure in the deposition chamber was about 5×10^{-8} mbar, and PLD was performed with an excimer laser KrF (LightMachinery, IPEX–742, λ=248 nm, pulse duration 25 ns) operated at a fluence of about 6 $J.cm^{-2}$. The target-substrate distance was fixed at 3.3 cm and during deposition, the substrate was heated from the backside by a halogen lamp in the temperature range 500°C–700°C.

Compositional and structural characterization was performed in a Scanning Electron Microscope (SEM) (LEO Gemini 1530 VP) equipped with energy dispersive spectroscopy (EDS) and x-ray diffraction (XRD) in a θ-2θ configuration (Cu-$K_{\alpha1}$ radiation-Bruker AXS D8 Advance). Cross-sectional SEM imaging was carried out on both cleaved and Focused Ion Beam (FIB) - cut (Ga ion beam, Crossbeam 550, Carl Zeiss Microscopy GmbH) samples. Magnetic hysteresis loops were measured at room temperature in a SQUID-VSM (Quantum Design MPMS 3) in a maximum applied field of 6.0 T. Atomic Force Microscopy (AFM) measurements were performed using a Dimension Icon AFM-BRUKER microscope. The microcantilever used was from AppNano (ACT probe, the nominal k = 34 N/m and f_o = 300 kHz).

III. Results and Discussion

A first set of films were prepared by deposition on substrates maintained at a temperature of 600°C, which is just under the reported crystallization temperature of the $Nd_2Fe_{14}B$ phase (630°C), and was shown to induce epitaxial out-of-plane oriented growth in NdFeB films prepared by PLD [16–18]. **Erreur ! Source du renvoi introuvable.** compares the average values of Nd/Fe atomic ratio, estimated from EDS analysis of typically ten thin films deposited from each composite target, with that measured on the targets themselves. The Nd/Fe ratio is

systematically lower in the films than in the corresponding target, dropping from 0.47 in the Nd richest target to 0.44 (average value) in the Nd richest films and from 0.18 in the Nd poorest target to 0.11 (average value) in the Nd-poorest films. The dashed line in **Erreur ! Source du renvoi introuvable.** corresponds to the expected film composition if the deposition process were congruent. The drop in Nd/Fe ratio from target to film may be attributed to differences in both the melting point of the concerned elements (Nd (1016°C) versus Fe (1538°C)), and their relative atomic mass (Nd: 144.24 g versus Fe: 55.85 g), the latter potentially affecting their distribution in the plasma plume and possibly leading to a redistribution of elements at the surface of the target. During laser-target interactions and film deposition, the constituent elements may slightly migrate, inducing local changes of the composition, as known for PLD [24]. It should be noted that the average Nd/Fe ratio in the Nd-poorest films is below the stoichiometric ratio of 0.14 of the $Nd_2Fe_{14}B$ phase.

Erreur ! Source du renvoi introuvable.a presents XRD patterns of representative samples of the films deposited at 600°C using the different targets. In all patterns, the Si(400) and Ta(110) peaks of the substrate and the buffer and capping layers are identified. Peaks of the $Nd_2Fe_{14}B$ phase are identified in all films, while reflections attributed to pure Nd (corresponding to (004) and (008) peaks) are identified in Nd-rich films (from target #1 - #3) and a peak of alpha-Fe (110) is identified in the Nd-poorest film (target #5). The relatively high intensities of the (*00l*) $Nd_2Fe_{14}B$ reflections compared to other reflections from this phase indicate preferential out of plane orientation. SEM images of cleaved cross sections of these films are shown in **Erreur ! Source du renvoi introuvable.**b. The film made from the target with the lowest Nd/Fe ratio (target #5) is predominantly composed of very fine equiaxed grains. Increasing the Nd/Fe ratio leads to bigger grains which become more and more elongated in films made from targets #4 and #3 and typically columnar in films made from targets #2 and #1. Most of the columnar grains traverse the film and are separated by some smaller equiaxed grains. AFM analysis performed at the surface of films (#1-#5) confirmed data obtained by SEM concerning the variation in grain size. The surface roughness of films (areas free of droplets) quantified by the root mean square (rms) roughness values increase by a factor of ~8 globally following the Nd/Fe atomic ratio (from about 4 nm to 33 nm for films with Nd/Fe = 0.11 to 0.42, respectively) (**Erreur ! Source du renvoi introuvable.**c), in agreement with the fact that the grain size also increases with Nd content.

Out-of-plane magnetic hysteresis loops of representative samples of the films deposited at 600°C using the different targets are compared in **Erreur ! Source du renvoi introuvable.**d. Note that the loops are not corrected for demagnetizing field effects, and the magnetization values are normalized. The film made from target #2 has both the highest values of coercivity (1.1 T) and remanence ratio M_{0T}/M_{6T} (0.91). All other films show very obvious two-phase or multi-phase behaviour. The films made from targets #1, #3 and #4 show comparable values of remanence ratio M_{0T}/M_{6T} (0.75). The coercivity drops to 0.9 T in the film made from target #1 and to 0.75 T in the films made from targets #3 and #4. The development of coercivity in films produced from targets #1–#4, which all have a Nd/Fe ratio higher than the $Nd_2Fe_{14}B$ phase, is attributed to the presence of a Nd-rich paramagnetic phase that serves to magnetically decouple $Nd_2Fe_{14}B$ grains. Relative variations in the coercivity values of these Nd-rich films may be attributed to differences in how the Nd-rich phase is distributed and the presence of secondary magnetic phases. While the sharpness of the hysteresis loop as it approaches coercivity is comparable in films made from targets #1 to #3, it is higher in the film made from target #4 and higher again in the Nd-poorest film made from target #5. The coercivity drops to just 0.2 T in the latter film, while the remanence ratio M_{0T}/M_{6T} drops to 0.2. These low values reflect the presence of alpha-Fe in this film, identified in XRD analysis and coherent with the Nd/Fe ratio of the film being less than that of the $Nd_2Fe_{14}B$ phase.

An SEM image of the FIB-cut cross section of a film made from target #2, is shown in **Erreur ! Source du renvoi introuvable.**a. Bright regions in the Nd-Fe-B layer, (one such region is identified by an orange arrow),

are attributed to the Nd-rich phase while the dark regions (e.g. the region identified by a white arrow), are attributed to the predominant $Nd_2Fe_{14}B$ phase. Based on image analysis of a number of such images, the volume content of the Nd-rich phase is estimated to be about 30 %. This value agrees very well with a value of 33 %, deduced from the average Nd/Fe atomic ratio measured by EDS analysis (**Erreur ! Source du renvoi introuvable.**) and considering the film to be composed of $Nd_2Fe_{14}B$ and pure Nd. An out-of-plane magnetic hysteresis loop of this sample is compared with an in-plane (ip) loop measured on the same sample (no demagnetizing field correction) in **Erreur ! Source du renvoi introuvable.**b. In this case, absolute values of magnetization, based on an estimate of the sample volume are represented on the y-axis. Note that the sample volume is calculated based on measurements of the film thickness and surface area and on a rough estimate of the volume of droplets, which are characteristic of metallic films made by PLD [21,25]. Droplets are estimated to account for ~ 25 vol% of the overall deposit. Extrapolating the ip and oop hysteresis loops leads to an intercept at about 8 T, which is comparable to the magnetocrystalline anisotropy of the $Nd_2Fe_{14}B$ phase (7.6 T). The lower value of remanence and higher value of high field slope of the ip measurement reflect the oop texture induced during film growth at 600°C. The error on the magnetization value, which is dominated by the error in volume estimation, is ~27 %. Indeed, an out-of-plane saturation magnetization value closer to 1 T can be expected for a well textured NdFeB film in which the hard magnetic $Nd_2Fe_{14}B$ phase accounts for 70 vol%. As the best magnetic properties were obtained for films produced with target #2, results reported hereafter concern films made with this target.

A set of films was made using target #2, in which the temperature of the substrate during deposition (T_d) was varied in the range 500°C-700°C. An EDS estimation of the Nd/Fe ratio for this series of thin films indicated very little variation of the Nd/Fe ratio (0.42 ± 0.01) between the films. XRD patterns of these films are compared in **Erreur ! Source du renvoi introuvable.**a. The degree of oop orientation of the NdFeB layer, reflected in the relative intensities of the (*00l*) peaks compared to other peaks of the $Nd_2Fe_{14}B$ phase, increases with increasing temperature up to 650°C. The intensities of $Nd_2Fe_{14}B$ and Nd peaks are greatly reduced in the film deposited at 700°C, and peaks of Nd_2O_3 are identified in the film. Peaks attributed to Ta_2O_3 are identified in films deposited at 630°C and above. Normalized oop hysteresis loops of this set of films are compared in **Erreur ! Source du renvoi introuvable.**b and the evolution of coercivity and remanence with deposition temperature are plotted in **Erreur ! Source du renvoi introuvable.**c. Relatively large error bars are associated with the $\mu_o M_r$ values, owing to the significant error in estimating the volume of these films, as discussed above. Films deposited between 550°C and 630°C have coercivity values in excess of 1 T, and comparable overall loop shape. The significantly lower value of coercivity of 0.5 T of the film deposited at 500°C is attributed to poor distribution of the Nd-rich grain boundary phase, resulting in poor decoupling of the $Nd_2Fe_{14}B$ grains. The drop in coercivity for films deposited at above 630°C is attributed to a combination of the evolution in microstructure (see below) and degradation of the film through oxidation. Initiation of oxidation at 650°C may not be visible using conventional XRD as it occurs over a very short range. The loop shape of the film deposited at 700°C is poorer than that deposited at 650°C, because of the greater extent of oxidation, as evidenced in the XRD patterns. This indicates that the base oxygen pressure of the PLD chamber used is too high to grow high quality Nd-Fe-B at temperatures of 650°C and above. A deposition temperature in the range 550°C–630°C favours both high coercivity and high remanence. The highest values of coercivity and remanence achieved in this study ($\mu_o H_c$ = 1.3 T and $\mu_o M_r$ > 1 T) are in the range of the best values reported for thin or thick films (e.g., Nd-Fe-B thick films fabricated by high deposition rate triode sputtering ($\mu_o H_c$ = 1.6 T and $\mu_o M_r$ = 1.4 T [23], $\mu_o H_c$ = 2.7 T and $\mu_o M_r$ = 1.15 T [26]). The coercivity values are intermediate while the remanence values are higher compared to films prepared by PLD with elemental targets ($\mu_o H_c$ = 2 T and $\mu_o M_r$ = 0.9 T [27]) and alloy targets ($\mu_o H_c$ = 0.72 T and $\mu_o M_r$ = 0.9 T [19,20,22]). Note that rare earth based films are susceptible to oxidation and the PLD of elemental targets cited above was carried out under UHV (10^{-9} mbar)

conditions. High deposition rates help to suppress oxidation of films deposited from alloy targets in chambers with a relatively poor base vacuum level, which is the case for the triode sputtered (18 µm/h, 10^{-6} mbar) and PLD with alloy target (40 µm/h, 10^{-6} mbar) films cited above. It is worth noting that while the base pressure of the chamber used here is better (10^{-7} mbar), the deposition rate is significantly lower (0.5 µm/h). Thus, the PLD system used here with an alloy target allows the fabrication of hard magnetic thin films and when combined with LNVS it has the potential to produce magnetic nanocomposites with soft inclusions of well controlled nm-size.

Plane-view SEM images of films showing distinct surface morphologies are shown in **Erreur ! Source du renvoi introuvable.**. The surface of the film deposited at T_d =500°C is characterized by "islands" of diameter up to 300 nm on an underlying layer with grains of diameter < 100 nm (**Erreur ! Source du renvoi introuvable.**a). The surface of the film deposited at T_d of 630°C is characterized by a high density of grains of size approaching 1 µm (**Erreur ! Source du renvoi introuvable.**b, identified by white arrows) some of which are separated by much smaller underlying grains of size 50-100 nm (identified by orange arrows). In the case of the film deposited at 650°C, connected platelet-like grains of size greater than 1 µm, with the plane of the platelets sometimes tilted with respect to that of the Si substrate, are identified, together with smaller grains of size close to 200 nm and an under-layer of grains of size 50-100 nm (**Erreur ! Source du renvoi introuvable.**c). AFM analysis indicates that the rms surface roughness increases from ~10 nm, for the film deposited at 500°C, to a maximum ~43 nm at 630 °C and then slightly reduces to ~35 nm at 700°C (**Erreur ! Source du renvoi introuvable.**). The maximum in rms roughness for the film deposited at 630°C followed by a drop at higher deposition temperatures is coherent with the compact isolated grains and inter-connected island (leading to a flatter surface in the same area of measurement) microstructures, respectively. The observed coarsening of the microstructure with increased deposition temperature may facilitate magnetization reversal through domain wall motion, which could contribute to a reduction of coercivity in the films deposited at higher temperatures.

IV. Conclusions

150 nm hard magnetic thin films of Nd-Fe-B were fabricated by PLD using a single ternary alloy target. The best magnetic properties were obtained for an Nd/Fe atomic target ratio of 0.45, a value far from that of 0.14 which corresponds to that of the $Nd_2Fe_{14}B$ phase. Films deposited on silicon substrates with buffer and capping layers of Ta at a temperature in the range of 550°C–630°C present the best hard magnetic properties, i.e. oop texture, coercivity values of up to 1.3 T, single magnetic phase behavior and a square loop shape. A Nd-rich phase corresponding to around 30 vol% of such films was revealed by structural (XRD, SEM, FIB-EBS) characterization. This phase, presumed to be paramagnetic, served to partially magnetically decouple $Nd_2Fe_{14}B$ grains, leading to the high coercivity values. Remanent magnetization values estimated to be close to 1 T validate these materials developed by PLD as a promising candidate for model materials to study certain aspects of magnetization reversal systems and for thin film magnet applications.

Acknowledgements

The authors thank the French National Research Agency (ANR) for financial support provided by the project ANR-SHAMAN 16-CE09-0019 project. This work benefited from technical support from the Common Service of Material Characterizations (CARMALIM) of the Université de Limoges. The authors gratefully acknowledge Richard Haettel and Frederico Orlando Keller from Institut Néel for fabricating the induction melted targets.

References

[1] J.M.D. Coey, Magnetism and Magnetic Materials, Cambridge Core. (2010). https://doi.org/10.1017/CBO9780511845000.

[2] O. Cugat, J. Delamare, G. Reyne, Magnetic micro-actuators and systems (MAGMAS), IEEE Transactions on Magnetics. 39 (2003) 3607–3612. https://doi.org/10.1109/TMAG.2003.816763.

[3] J. Pivetal, D. Royet, G. Ciuta, M. Frenea-Robin, N. Haddour, N.M. Dempsey, F. Dumas-Bouchiat, P. Simonet, Micro-magnet arrays for specific single bacterial cell positioning, Journal of Magnetism and Magnetic Materials. 380 (2015) 72–77. https://doi.org/10.1016/j.jmmm.2014.09.068.

[4] M. Sagawa, S. Fujimura, N. Togawa, H. Yamamoto, Y. Matsuura, New material for permanent magnets on a base of Nd and Fe (invited), Journal of Applied Physics. 55 (1984) 2083–2087. https://doi.org/10.1063/1.333572.

[5] J.J. Croat, J.F. Herbst, R.W. Lee, F.E. Pinkerton, Pr-Fe and Nd-Fe-based materials: A new class of high-performance permanent magnets (invited), Journal of Applied Physics. 55 (1984) 2078–2082. https://doi.org/10.1063/1.333571.

[6] R. Skomski, J.M.D. Coey, Giant energy product in nanostructured two-phase magnets, Phys. Rev. B. 48 (1993) 15812–15816. https://doi.org/10.1103/PhysRevB.48.15812.

[7] T.P. Yadav, R.M. Yadav, D.P. Singh, Mechanical Milling: a Top Down Approach for the Synthesis of Nanomaterials and Nanocomposites, Nanoscience and Nanotechnology. 2 (2012) 22–48.

[8] D.W. Hu, M. Yue, J.H. Zuo, R. Pan, D.T. Zhang, W.Q. Liu, J.X. Zhang, Z.H. Guo, W. Li, Structure and magnetic properties of bulk anisotropic SmCo5/α-Fe nanocomposite permanent magnets prepared via a bottom up approach, Journal of Alloys and Compounds. 538 (2012) 173–176. https://doi.org/10.1016/j.jallcom.2012.05.079.

[9] V. Dupuis, G. Khadra, A. Hillion, A. Tamion, J. Tuaillon-Combes, L. Bardotti, F. Tournus, Intrinsic magnetic properties of bimetallic nanoparticles elaborated by cluster beam deposition, Phys. Chem. Chem. Phys. 17 (2015) 27996–28004. https://doi.org/10.1039/C5CP00943J.

[10] R. Alayan, L. Arnaud, A. Bourgey, M. Broyer, E. Cottancin, J.R. Huntzinger, J. Lermé, J.L. Vialle, M. Pellarin, G. Guiraud, Application of a static quadrupole deviator to the deposition of size-selected cluster ions from a laser vaporization source, Review of Scientific Instruments. 75 (2004) 2461–2470. https://doi.org/10.1063/1.1764607.

[11] V. Dupuis, G. Khadra, S. Linas, A. Hillion, L. Gragnaniello, A. Tamion, J. Tuaillon-Combes, L. Bardotti, F. Tournus, E. Otero, P. Ohresser, A. Rogalev, F. Wilhelm, Magnetic moments in chemically ordered mass-selected CoPt and FePt clusters, Journal of Magnetism and Magnetic Materials. 383 (2015) 73–77. https://doi.org/10.1016/j.jmmm.2014.12.061.

[12] M. Gaudin, P. Carles, E. Laborde, C. Champeaux, F. Dumas-Bouchiat, A dual nanosecond-pulsed laser setup for nanocomposite synthesis—Ag nanoparticles in Al2O3/VO2 matrix, Journal of Applied Physics. 125 (2019) 054301. https://doi.org/10.1063/1.5058107.

[13] F. Dumas-Bouchiat, H.S. Nagaraja, F. Rossignol, C. Champeaux, A. Catherinot, Magnetic domains in Co-cluster assembled films deposited by LECBD, Applied Surface Science. 247 (2005) 76–82. https://doi.org/10.1016/j.apsusc.2005.01.036.

[14] F. Dumas-Bouchiat, H.S. Nagaraja, F. Rossignol, C. Champeaux, G. Trolliard, A. Catherinot, D. Givord, Cobalt cluster-assembled thin films deposited by low energy cluster beam deposition: Structural and magnetic investigations of deposited layers, Journal of Applied Physics. 100 (2006) 064304. https://doi.org/10.1063/1.2335670.

[15] A. Fischer, R. Kruk, D. Wang, H. Hahn, Magnetic properties of iron cluster/chromium matrix nanocomposites, Beilstein J. Nanotechnol. 6 (2015) 1158–1163. https://doi.org/10.3762/bjnano.6.117.

[16] A.R. Kwon, S. Fähler, V. Neu, L. Schultz, Effect of composition on phase formation, microstructure and magnetic properties of Nd–Fe–B thin films, Journal of Magnetism and Magnetic Materials. 302 (2006) 252–258. https://doi.org/10.1016/j.jmmm.2005.09.014.

[17] U. Hannemann, S. Fähler, S. Oswald, B. Holzapfel, L. Schultz, Effect of Cr and Ta buffers on hard magnetic Nd2Fe14B films, Journal of Magnetism and Magnetic Materials. 242–245 (2002) 1294–1296. https://doi.org/10.1016/S0304-8853(01)01266-5.

[18] V. Neu, S. Melcher, U. Hannemann, S. Fähler, L. Schultz, Growth, microstructure, and magnetic properties of highly textured and highly coercive Nd-Fe-B films, Phys. Rev. B. 70 (2004) 144418. https://doi.org/10.1103/PhysRevB.70.144418.

[19] M. Nakano, S. Sato, H. Fukunaga, F. Yamashita, A method of preparing anisotropic Nd–Fe–B film magnets by pulsed laser deposition, Journal of Applied Physics. 99 (2006) 08N301. https://doi.org/10.1063/1.2159411.

[20] M. Nakano, K. Takashima, A. Yamashita, T. Yanai, H. Fukunaga, Relationship between target materials and various properties of PLD-made isotropic Nd-Fe-B films, Journal of Magnetism and Magnetic Materials. 502 (2020) 166557. https://doi.org/10.1016/j.jmmm.2020.166557.

[21] P. Zheng, Y. Haik, C.-J. Chen, Z. Jiang, J.P. Zheng, Properties of NdFeB film grown on silicon substrate by PLD under external magnetic field, Surface and Coatings Technology. 194 (2005) 372–377. https://doi.org/10.1016/j.surfcoat.2004.11.033.

[22] M. Nakano, Y. Chikuba, M. Oryoshi, A. Yamashita, T. Yanai, R. Fujiwara, T. Shinshi, H. Fukunaga, Nd–Fe–B Film Magnets With Thickness Above 100 μm Deposited on Si Substrates, IEEE Transactions on Magnetics. 51 (2015) 1–4. https://doi.org/10.1109/TMAG.2015.2438099.

[23] N.M. Dempsey, A. Walther, F. May, D. Givord, K. Khlopkov, O. Gutfleisch, High performance hard magnetic NdFeB thick films for integration into micro-electro-mechanical systems, Appl. Phys. Lett. 90 (2007) 092509. https://doi.org/10.1063/1.2710771.

[24] E. Toyserkani, N. Rasti, Ultrashort pulsed laser surface texturing, in: J. Lawrence, D.G. Waugh (Eds.), Laser Surface Engineering, Woodhead Publishing, 2015: pp. 441–453. https://doi.org/10.1016/B978-1-78242-074-3.00018-0.

[25] E. van de Riet, C.J.C.M. Nillesen, J. Dieleman, Reduction of droplet emission and target roughening in laser ablation and deposition of metals, Journal of Applied Physics. 74 (1993) 2008–2012. https://doi.org/10.1063/1.354763.

[26] N.M. Dempsey, T.G. Woodcock, H. Sepehri-Amin, Y. Zhang, H. Kennedy, D. Givord, K. Hono, O. Gutfleisch, High-coercivity Nd–Fe–B thick films without heavy rare earth additions, Acta Materialia. 61 (2013) 4920–4927. https://doi.org/10.1016/j.actamat.2013.04.055.

[27] U. Hannemann, S. Fähler, V. Neu, B. Holzapfel, L. Schultz, Intrinsic and extrinsic properties of epitaxial Nd2Fe14B films, Appl. Phys. Lett. 82 (2003) 3710–3712. https://doi.org/10.1063/1.1576913.

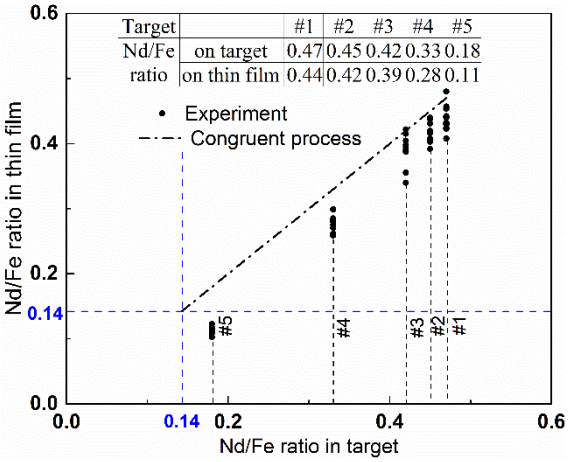

Figure 1: Nd/Fe atomic ratios of targets versus Nd/Fe atomic ratio of films; Ta/Nd-Fe-B/Ta films deposited by PLD at T_d = 600°C and ~ 6 J.cm^{-2} on Si/SiO_2 substrates. Black dash-dotted line represents a perfect congruent transfer.

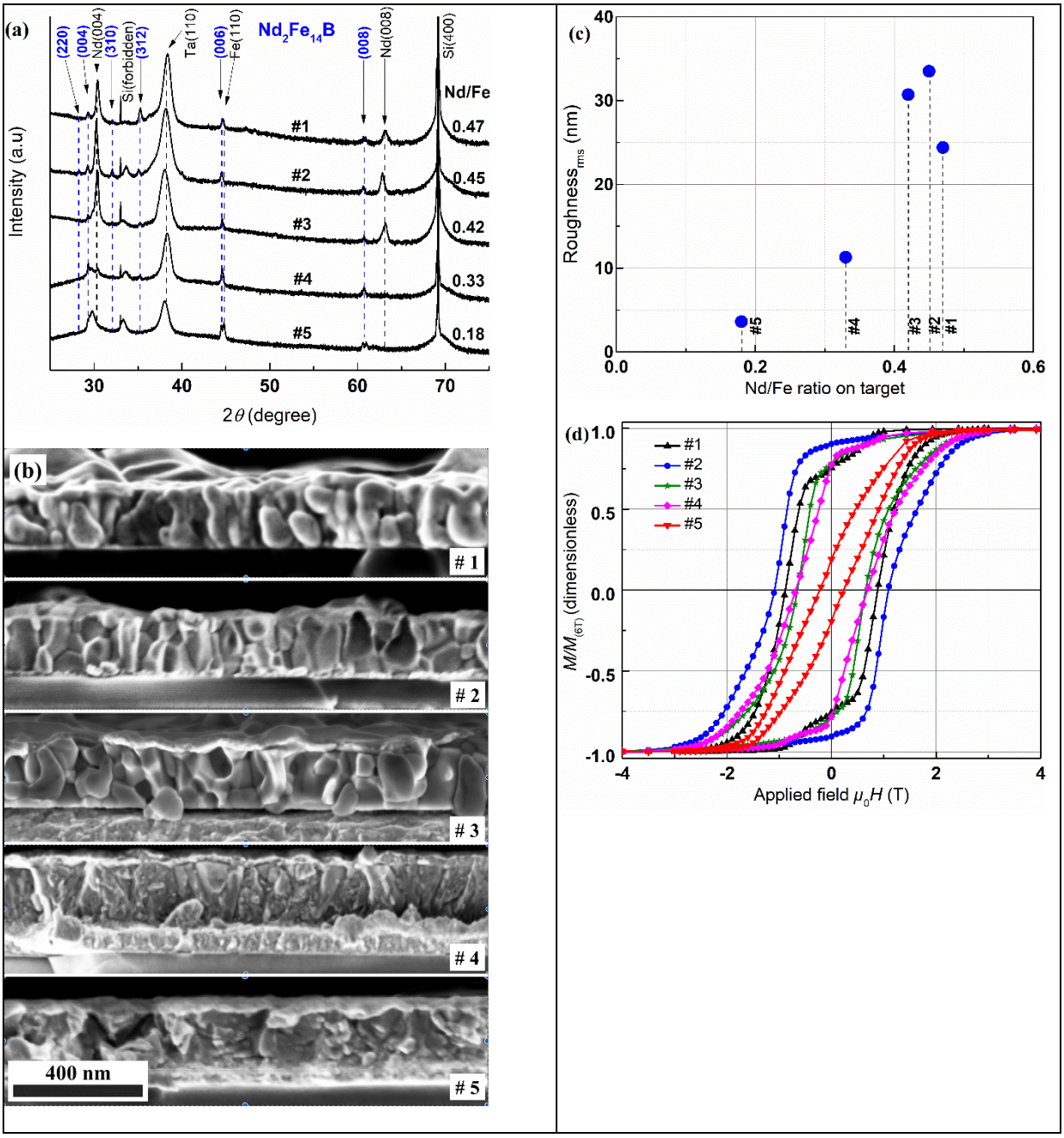

Figure 2: Characterization of Ta/Nd-Fe-B(150 nm)/Ta films deposited at 600°C on Si/SiO_2 substrates (a) XRD patterns of thin films made from the five different targets; (b) SEM images of the fractured cross sections of films from the five targets; (c) AFM rms surface roughness; and (d) Out-of-plane magnetic hysteresis loops (uncorrected for demagnetization field and normalised) of films deposited from the five targets.

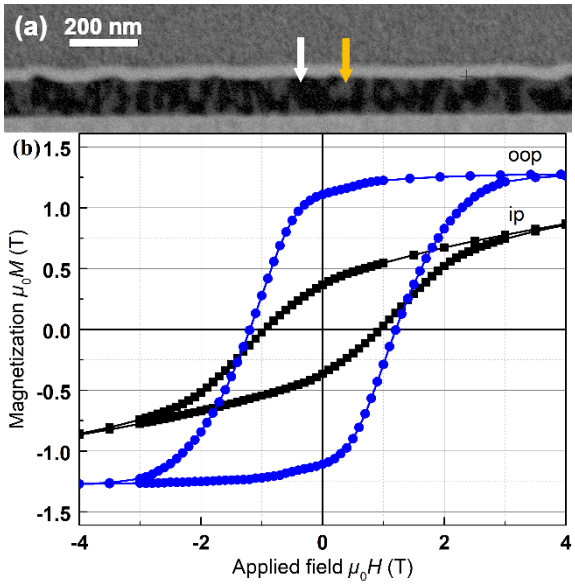

Figure 3: Characterization of the film made from target #2 deposited at 600°C on Si/SiO_2. (a) FIB-EBS cross-sectional images in which $Nd_2Fe_{14}B$ grains elongated in the *z* direction (black regions, one of which is identified by a white arrow) are found together with a Nd rich phase (gray regions, one of which is identified by an orange arrow); and (b) in-plane (ip) and out-of-plane (oop) magnetic hysteresis loops (uncorrected for demagnetization field).

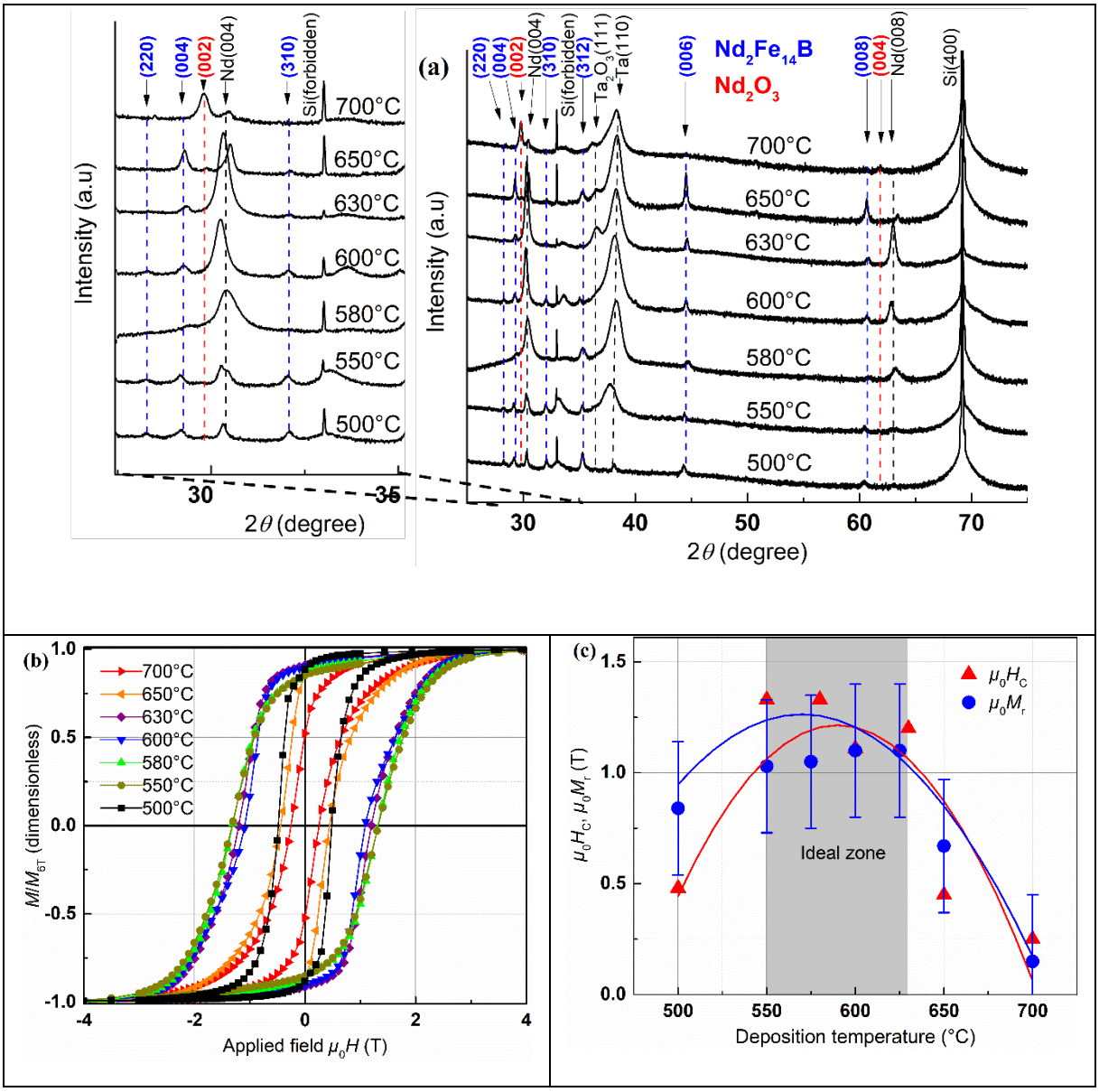

Figure 4: The evolution in structural and magnetic properties of Ta/Nd-Fe-B/Ta thin films on Si/SiO_2 substrates made from target #2 as a function of deposition temperatures-T_d ranging from 500°C to 700°C. (a) XRD diffractograms of the thin films with an enlarged range from 25° to 35°; (b) oop magnetic hysteresis loops (uncorrected for demagnetization field and normalized); and (c) coercivity ($\mu_o H_c$) and remanent magnetization ($\mu_o M_r$) together with curves representing guides to the eye.

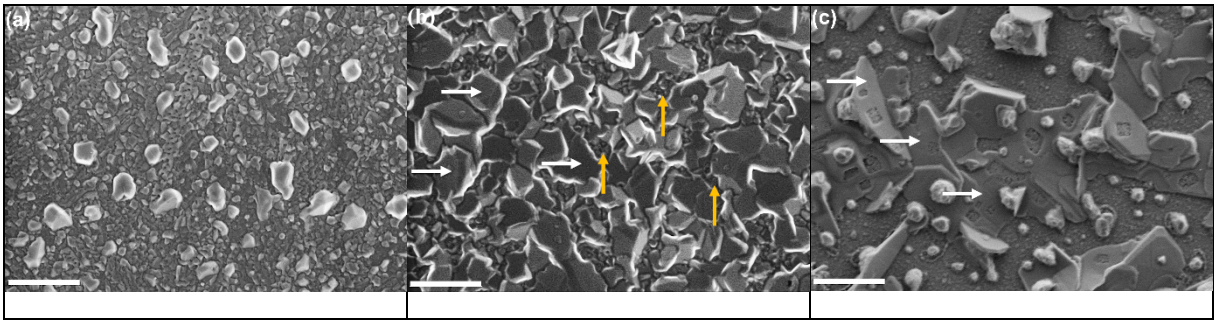

Figure 5: Plane-view SEM images showing the distinct surface microstructures of Ta/Nd-Fe-B/Ta films deposited at T_d (a) 500°C; (b) 630°C; and (c) 650°C. The scale bar in all images is 1µm.

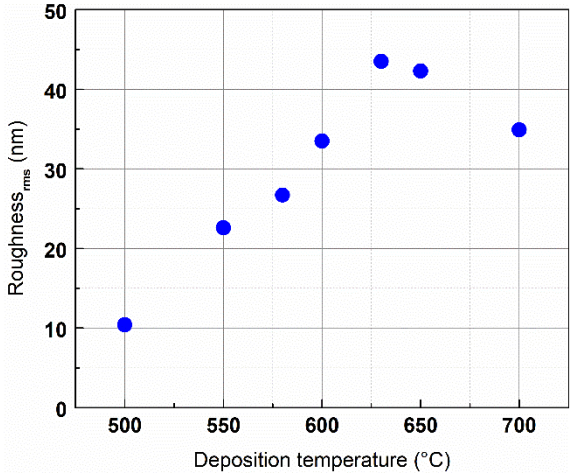

Figure 6: The AFM rms surface roughness of Ta/Nd-Fe-B/Ta films from target #2 as a function of deposition temperatures-T_d.